Polyhedron 48 (2012) 181–188

Contents lists available at SciVerse ScienceDirect

Polyhedron

journal homepage: www.elsevier.com/locate/poly

Ni(II), Pd(II) and Cu(II) complexes with *N*-(dialkylthiocarbamoyl)-*N*′-picolylbenzamidines: Structure and activity against human MCF-7 breast cancer cells

Hung Huy Nguyen [a,*], Canh Dinh Le [b], Chien Thang Pham [a], Thi Nguyet Trieu [a], Adelheid Hagenbach [c], Ulrich Abram [c,*]

[a] Department of Chemistry, Hanoi University of Science, 19 Le Thanh Tong, Hanoi, Viet Nam
[b] Department of Chemistry, Quy Nhon University, 170 An Duong Vuong, Quy Nhon, Viet Nam
[c] Institute of Chemistry and Biochemistry, Freie Universität Berlin, Fabeckstraße 34-36, D-14195 Berlin, Germany

ARTICLE INFO

Article history:
Received 18 May 2012
Accepted 28 August 2012
Available online 23 September 2012

Keywords:
Tridentate ligands
Thiocarbamoyl benzamidines
Cytotoxicity
Ni(II) complex
Pd(II) complex
Cu(II) complex

ABSTRACT

N-(Dialkylthiocarbamoyl)-*N*′-picolylbenzamidines (HL^{Et} and HL^{Morph}) react with $NiCl_2$, $CuCl_2$ and $[PdCl_2(MeCN)_2]$ with the formation of complexes of the general composition $[M(L^R)Cl]$ (M = Ni (**1**), Pd (**2**)) and the dimeric complexes $[\{Cu(L^R)Cl\}_2]$ (**3**). The molecular structures of complexes **1** and **2** exhibit a square-planar coordination sphere, in which the organic ligands coordinate in a *S,N,N* coordination mode. The two subunits of **3**, the arrangement of each is similar to those of **1** and **2**, are connected via two weak Cu–Cl′ bonds. The copper complexes $[\{Cu(L^R)Cl\}_2]$ (**3**) are slowly oxidized under aerobic conditions to give $[\{Cu(^*L^R)Cl\}_2]$ complexes (**4**), where H^*L^R = N-(dialkylthiocarbamoyl)-N′-picolinoyl-benzamidines. Complexes **1** and **2** show a very weak reduction of the growth of human MCF-7 breast cancer cells. Complexes **4**, however, possess a remarkable cytotoxicity with IC_{50} values within the range 0.40–1.05 μM. Compounds **3** are likely converted to **4** under the conditions of the cytotoxicity assay, and consequently exhibit IC_{50} values very similar to those found for **4**.

1. Introduction

Bidentate *N*-(dialkylthiocarbamoyl)benzamidines (*S,N*-type ligands of Scheme 1) (**I**) are well known chelators, which can be readily prepared by the reactions of *N*-(dialkylthiocarbamoyl) benzimidoylchlorides with ammonia or primary amines [1,2]. During recent decades, a large number of bidentate benzamidine ligands and their complexes with most transition metal ions have been extensively studied [3]. In principle, thiocarbamoylbenzamidines with higher denticity can readily be achieved by the introduction of functionalized primary amines into the ligand synthesis. However, surprisingly less is known about the chemistry of such multidentate benzamidine-type ligands. Only a few tridentate benzamidines having *S,N,N* [4], *S,N,O* [4–6], *S,N,S* [7,8] and *S,N,P* [9] donor sets (**II**) and a tetradentate benzamidine with an *S,N,N,S* donor set [10] (Scheme 1) (**III**) have been recently reported. The coordination chemistry of these ligands is mainly restricted to their rhenium and technetium complexes [4–9]. For other transition metals, hitherto, there are only reports about two complexes of Cu(II) and Ni(II) with tetradentate benzamidines derived from o-phenylenediamine [10] and a few complexes of Au(III) with tridentate benzamidines derived from 4,4-dialkylthiosemicarbazide [11].

Recently, we have pursued investigations on the biological activitiy of multidentate benzamidines and their transition metal complexes. In fact, derivatives of thiosemicarbazides and their $\{Re^{V}O\}^{3+}$ and Au(III) complexes were found promising for the inhibition of the growth of human MCF-7 breast cancer cells [8,11]. Additionally, it is evident that the properties of the compounds can easily be tuned by convenient modifications to the periphery of their chelating systems, which allows systematic SAR studies [4–11]. Here, we report on the synthesis and characterization of complexes of potentially tridentate *N*-(dialkylthiocarbamoyl)-*N*′-picolyl benzamidine ligands (HL^R, Chart 1) with transition metal ions such as Ni(II), Pd(II) and Cu(II), as well as the first evaluation of their *in vitro* cytotoxic activity.

2. Results and discussion

N-(Dialkylthiocarbamoyl)-*N*′-picolyl benzamidines readily react with $NiCl_2$ in MeOH to give red solutions, from which red crystals of the composition $[Ni(L^R)Cl]$ (**1**) were isolated in high yields (Scheme 2).

* Corresponding authors. Address: Department of Inorganic Chemistry, Hanoi University of Science, 19 Le Thanh Tong, Hanoi, Viet Nam (H.H. Nguyen). Tel.: +84 1294849543; fax: +84 43 8241140.
E-mail addresses: nguyenhunghuy@hus.edu.vn (H.H. Nguyen), abram@chemie.fu-berlin.de (U. Abram).

0277-5387/$ - see front matter © 2012 Elsevier Ltd. All rights reserved.
http://dx.doi.org/10.1016/j.poly.2012.08.088

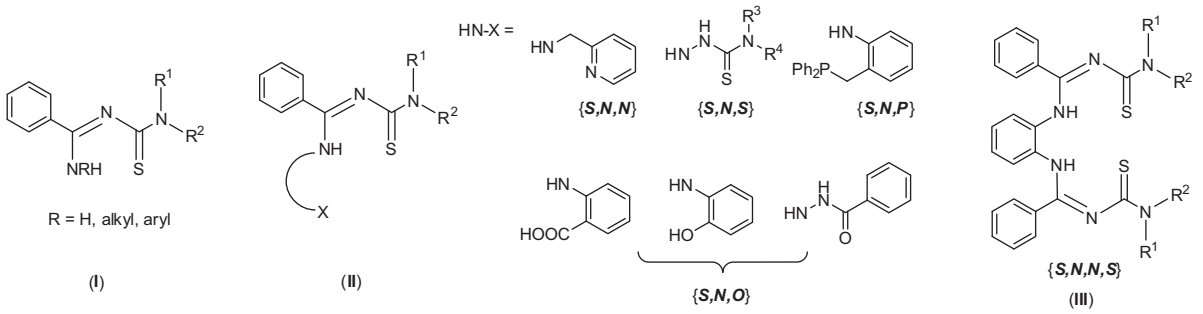

Scheme 1. Bi- tri- and tetradentate thiocarbamoyl benzamidines.

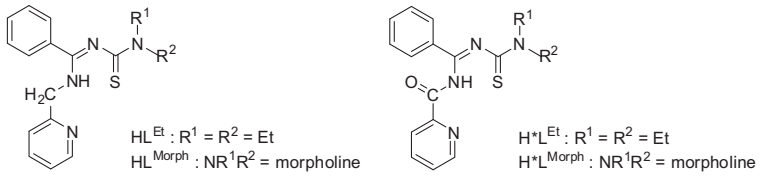

Chart 1. Ligands used in this study.

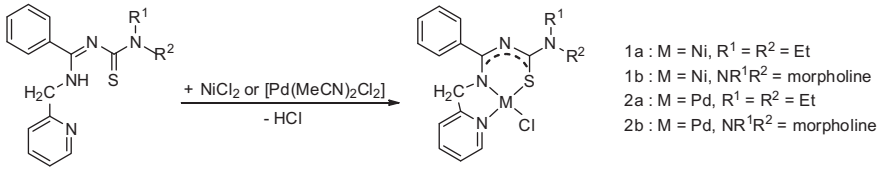

Scheme 2. Synthesis of [Ni(L^R)Cl] (**1**) and [Pd(L^R)Cl] (**2**).

IR spectra of complexes **1** exhibit strong bands in the 1500 cm^{-1} region, but no absorptions in the range between 1608 and 1620 cm^{-1}, where the $\nu_{C=N}$ stretches in the spectra of the non-coordinated benzamidines typically appear. This corresponds to a strong bathochromic shift of about 110 cm^{-1} and reflects chelate formation with a large degree of π-electron delocalization within the chelate rings, as has been observed for other benzamidine complexes [3]. The absence of absorption bands in the region around 3215 cm^{-1}, which are assigned to ν_{N-H} vibrations in the uncoordinated HL, indicates the expected deprotonation of the ligands upon complex formation.

^{1}H NMR spectra of **1** are characterized by broad signals for most of the protons. The hindered rotation around the R_2N–CS bonds, commonly discussed in ^{1}H NMR studies of related complexes, may cause the poor resolution of the signals corresponding to the aliphatic protons in the dialkylamino groups [12]. However, the described pattern is most likely due to the labile character and/or distortion of the square planar Ni(II) complexes since the broadening is extended to the signals of the aromatic protons in the phenyl as well as in the pyridyl rings [13]. Nevertheless, the rigid model of the R_2N–CS moiety, which results in magnetic inequivalence of the alkyl groups, is also found in the spectra of the Ni(II) complexes under study. Thus, in the ^{1}H NMR spectrum of **1a**, four broadened singlets, two in the region of 1.0–1.2 ppm and two others in the region around 3.6 ppm are assigned to the resonances of CH_3 and NCH_2 protons, respectively. The resonances corresponding to the four methylene groups of the Morph residue in **1b** are observed as four broad signals between 3.7 and 4.2 ppm. More importantly, the absence of the broad N–H resonance, found in the region of 6.9 ppm for the free ligands, in the ^{1}H NMR spectra of **1** confirms the deprotonation of the coordinated benzamidines and formation of {*N,S*} chelate rings. An additional coordination bond between the central Ni atom and the pyridine N atom is indicated by a significant low field shift of about 0.4 ppm of the signal assigned to the proton in the *ortho* position to this N atom. This consequently leads to a five-membered chelate ring and results in a high field shift about 0.3 ppm of the resonance corresponding to the two methylene protons in the ring. Furthermore, the observation of a singlet for the CH_2 protons of the five-membered chelate ring reveals their magnetic equivalence, which is consistent with a square-planar coordination environment for the Ni(II) complexes. In contrast, in octahedral complexes of $\{Re^{V}O\}^{3+}$, these two methylene protons are magnetically unequal. Their resonances are observed as two doublets with typical geminal coupling patterns [4].

The proposed composition and structure of the complexes **1**, derived from spectroscopic analysis, are supported by X-ray single crystal diffraction studies. The molecular structure of **1b** is shown in Fig. 1 as a representative for this type of complex. Because the structure of **1a** is identical, with the exception of the dialkylamino residue, no extra Figure is given. Table 1 contains selected bond lengths and angles for both compounds. In both complexes, the Ni atom reveals the expected square-planar environment. Three positions in the coordination sphere are occupied by the S1, N5, N56 donor atoms of the monoanionic $\{L^R\}^-$ ligand and the remaining position is occupied by a chlorido ligand. The formed square planes are slightly distorted with maximum deviations of 0.045(1) and 0.038(1)/0.065(1) Å from the mean least-square plane for the N5 atoms in **1a** and **1b**, respectively. The Ni-N5 bonds are slightly shorter (about 0.06 Å) than the Ni-N56 bonds. This is in good agreement with the expected deprotonation of the ligands and the formation of mononanionic benzamidine chelate rings. Nevertheless, all the Ni-N and Ni-S bond lengths are in the typical ranges found for nickel–nitrogen and nickel–sulfur single bonds. In both complexes, the six-membered benzamidine chelate rings are

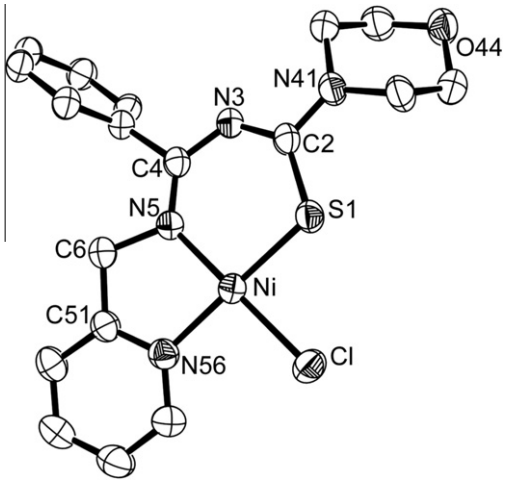

Fig. 1. ORTEP representation of **1b** (50% thermal ellipsoids) [22]. Hydrogen atoms have been omitted for clarity.

Table 1
Selected bond lengths and angles in [Ni(L^{Et})Cl] (**1a**), [Ni(L^{Mor})Cl] (**1b**) and [Pd(L^{Et})Cl] (**2a**).

	1a	1b*	2a*
Bond lengths (Å)			
M–S1	2.136(1)	2.137(1)/2.138(1)	2.228(3)/2.233(3)
M–N5	1.868(2)	1.875(2)/1.868(2)	1.981(7)/1.976(6)
M–N56	1.928(2)	1.944(2)/1.942(2)	2.042(8)/2.048(8)
M–Cl	2.196(1)	2.212(1)/2.193(1)	2.325(2)/2.315(2)
S1–C2	1.733(3)	1.717(3)/1.714(3)	1.722(8)/1.732(8)
C2–N3	1.339(3)	1.330(3)/1.333(3)	1.34(1)/1.32(1)
N3–C4	1.332(3)	1.342(3)/1.340(3)	1.34(1)/1.33(1)
C4–N5	1.316(3)	1.312(4)/1.315(4)	1.29(1)/1.33(1)
C2–N41	1.340(3)	1.354(4)/1.359(4)	1.34(1)/1.35(1)
Angles (°)			
S1–M–N5	95.6(1)	95.5(1)/95.9(1)	95.9(2)/96.2(2)
N5–M–N56	85.1(1)	85.6(1)/86.1(1)	83.2(3)/82.7(3)
N56–M–Cl	94.0(1)	94.1(1)/93.5(1)	94.6(2)/94.2(2)
Cl–M–S1	85.3(1)	84.8(1)/84.6(1)	86.3(1)/87.0(1)
S1–M–N56	179.4(1)	178.5(1)/175.5(1)	179.0(2)/178.6(2)
N5–M–Cl	175.8(1)	177.3(1)/177.4(1)	175.9(2)/176.6(2)

* Two crystallographically independent species.

slightly distorted, with main deviations of 0.184(1) Å (for S1 in **1a**) and 0.094(1)/0.099(1) Å (for Ni in **1b**) from the mean least-square planes. A considerable delocalization of π-electron density inside the chelate rings is observed and indicated by the C–S and C–N bond lengths, which are all within the range between typical C–S (1.80 Å), C–N (1.47 Å) single bonds and C=S (1.67 Å), C=N (1.28 Å) double bonds [14]. The bond length equalization is even extended to the C2–N41 bonds, which are significantly shorter than that expected for single bonds. This observation is consistent with the hindered rotation around the CS–NR_2 bond, as revealed by the ^{1}H NMR analysis.

Reactions of HL^R with [$PdCl_2(MeCN)_2$] in CH_2Cl_2/MeOH (Scheme 2) are much slower than those with $NiCl_2$. The addition of a supporting base like Et_3N accelerates the reaction rate, which can be detected by a rapid color change from brown–yellow to bright yellow. Crystalline yellow solids of the composition [Pd(L^R)Cl] (**2**) are isolated as the sole products in excellent yields.

The IR spectra of complexes **2** are very similar to those of **1**, except that the absorption bands of the $\nu_{C=N}$ stretches appear at higher frequencies by about 10 cm^{-1}. The ^{1}H NMR spectra of **2** exhibit a compatible pattern, but with a better resolution. In the case of **2a**, for instance, the hindered rotation around the CS–NEt_2 bond also results in two magnetically unequal ethyl groups, which is indicated by well resolved signals including two triplets and two other quartets with almost the same chemical shifts as the corresponding resonances in **1a**. The most significant differences are the resonances corresponding to the proton in the ortho position to the pyridine N atom and the methylene protons in $PyCH_2$–. These signals are low field shifted by approx. 0.3 ppm in the ^{1}H NMR spectra of **2** compared to those of complexes **1**.

Compounds **2** are well soluble in chlorinated solvents like $CHCl_3$ and CH_2Cl_2, but almost insoluble in alcohols. Slow evaporation of a CH_2Cl_2/MeOH solution of **2a** gave single crystals suitable for X-ray studies. An ORTEP diagram of **2a** (Fig. 2) confirms an analogous bonding situation as discussed for complexes **1**. The corresponding bond lengths and angles are compared to those of the structurally characterized nickel complexes in Table 1. The coordination sphere of the palladium atom is best described as almost ideal square-planar, with a main distortion of only 0.046(1)/0.021(1) Å for atom N5 from the mean least-squares plane formed by the Pd, S1, N5, N56 and Cl atoms. The planar feature can be extended to include both the six-membered benzamidine ring and the five-membered ring, with a maximum deviation from the mean least-squares plane of 0.103(3)/0.091(3) Å for atom S1.

The reactions of the ligands HL^R and $CuCl_2$ in MeOH lead to the rapid formation of dark blue microcrystalline solids of the composition [{Cu(L^R)Cl}$_2$] (**3**) (Scheme 3). IR spectra of complexes **3**, which mainly exhibit the same patterns as described for the nickel complexes **1**, indicate a similar bonding situation as discussed for the nickel complexes. Compounds **3** are stable in the solid state. Solutions of **3** in CH_2Cl_2/MeOH, however, gradually change their color from blue to light blue under aerobic conditions. Thus, X-ray quality single crystals of **3a** could only be obtained by slow diffusion of MeOH into a CH_2Cl_2 solution of the complex under N_2 atmosphere. Fig. 3 illustrates the dimeric structure of the compound. Selected bond lengths and angles of the two crystallographically independent molecules found in the asymmetric unit cell of **3a** are summarized in Table 2. In each monomer, the arrangement of the organic ligand and the chlorido ligand around the central copper atom is analogous to those described for the Ni(II) and Pd(II) complexes. The two subunits, which are related by a center of inversion, are connected by two very weak Cu-Cl′ bonds with the distances of 2.978(1)/2.947(1) Å for the two symmetry-independent molecules. Thus, each of the copper atoms has a distorted square pyramidal environment (Addison distortion index, τ = 0.11/0.12) with the distance from the central atom to the apical

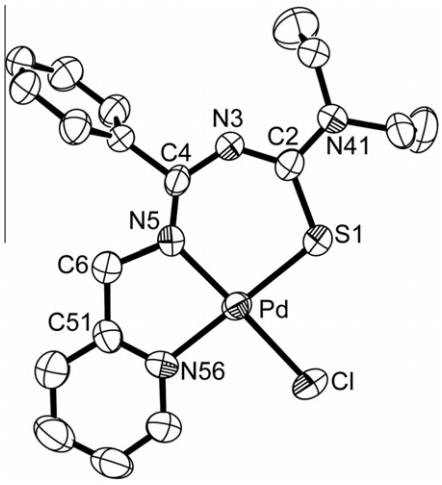

Fig. 2. ORTEP representation of **2a** (50% thermal ellipsoids) [22]. Hydrogen atoms have been omitted for clarity.

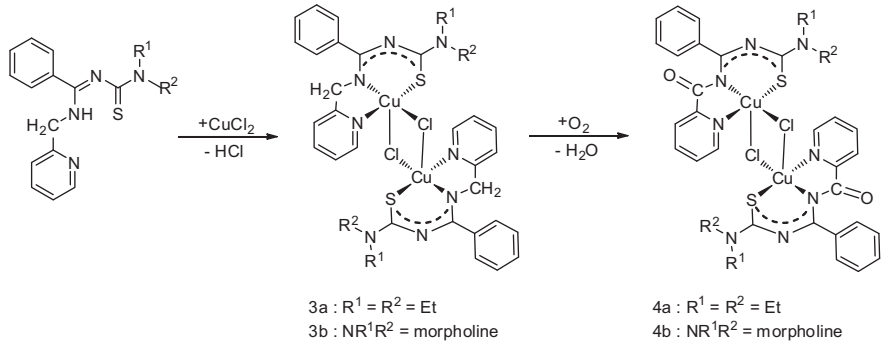

Scheme 3. Synthesis of $[\{Cu(L^R)Cl\}_2]$(**3**) and $[\{Cu(^*L^R)Cl\}_2]$(**4**).

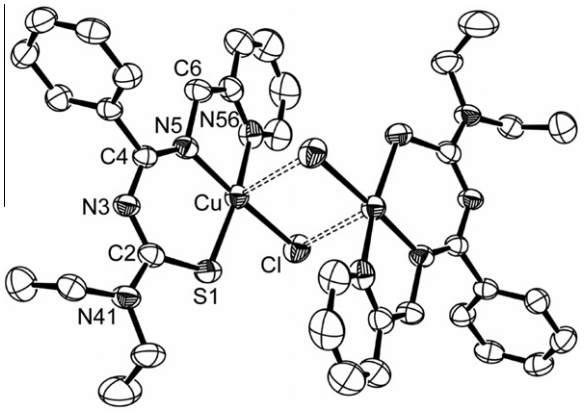

Fig. 3. ORTEP representation of **3a** (50% thermal ellipsoids) [22]. Hydrogen atoms have been omitted for clarity.

position being much elongated. Although the basal plane of **3a** is distorted, the central Cu atom is displaced from the plane of the four in-plane donor atoms by only 0.083(1)/0.087(1) Å toward the axial ligand. This distance is not in the common range (0.1–0.5 Å) for square-pyramidal Cu(II) complexes, but is consistent with the previously reported inverse correlation between the deviation out of the basal plane and the distance to the apical donor atom (L5) of a central Cu atom, i.e. the longer the Cu–L5 distance the smaller the deviation [15].

The electronic spectra of **3** in $CHCl_3$ show a broad band centered at 575 nm with low extinction coefficient values that correspond to the *d–d* transition. These absorption bands are in the same region reported for distorted square pyramidal $[Cu\{N_2S\}Cl_2]$ complexes having a similar ligand sphere, such as $[Cu(HL)Cl_2]$ complexes where HL are {N,N,S} tridentate, 2-pyridineformamide N(4)-dialkylthiosemicarbazone [16]. ESI(+) mass spectra of **3** show no molecular peak for the dimeric structure, but peaks of moderate intensity are obtained which can be assigned to the monomeric ions $[Cu(L^R)Cl+H]^+$ (*m/z* = 424 for **3a**, *m/z* = 438 for **3b**) with the expected isotopic patterns. More intense peaks are assigned to $[Cu(L^R)]^+$ fragments, which result from the loss of the chlorido ligands from the monomeric ions.

Slow evaporation of a CH_2Cl_2/MeOH solution of **3** in air results in the formation of light blue crystals of **4**. The IR spectra of these compounds are characterized by a very strong absorption band in the 1660 cm^{-1} region. Such bands are indicative of $\nu_{C=O}$ stretches, which is a strong hint for the oxidation of the main skeleton of the organic ligands$\{L^R\}^-$ by atmospheric oxygen and the formation of an amide. This assumption is supported by the ESI(+) mass spectra of **4**. They show the same fragmentation pattern as the corresponding complexes **3**, but at *m/z* values, which are each higher by 14 mass units. The visible spectra of **4** reveal a single band in the 600 nm region. This corresponds to a red shift of about 25 nm compared to the corresponding bands of **3** and reflects a smaller elongation of the coordination sphere toward the *z* axis [17].

An X-ray structural study confirmed the expected oxidation of the ligand $\{L^R\}^-$, in which the methylene group attached to the pyridine ring was converted to a carbonyl group to form a new tridenate monoanionic ligand $\{^*L^R\}^-$. The described air oxidation of the benzylic carbon in HL^R is unprecedented. In the solid state, compounds **4** are also in a dimeric form, with the general composition $[\{Cu(^*L^R)Cl\}_2]$. The dimerization in **4a** (Fig. 4) is very similar to that in **3a** except that the coordination bond between the central Cu(II) atom and the axial chlorido ligand is about 0.3 Å shorter. This results in an increase of the deviation of central Cu atom out of the

Table 2
Selected bond lengths and angles in $[\{Cu(^*L^{Et})Cl\}_2]$ (**3a**) and $[\{Cu(^*L^{Et})Cl\}_2]$ (**4a**).

Bond lengths (Å)	**3a***	**4a**		**3a***	**4a**
Cu–S1	2.224(1)/2.227(1)	2.286(1)	S1–C2	1.716(3)/1.719(3)	1.726(5)
Cu–N5	1.948(2)/1.941(2)	1.956(4)	C2–N3	1.344(4)/1.341(4)	1.358(6)
Cu–N56	2.028(2)/2.030(3)	2.040(3)	C2–N41	1.342(4)/1.353(4)	1.322(5)
Cu–Cl	2.276(1)/2.271(1)	2.289(1)	N3–C4	1.335(4)/1.344(3)	1.294(5)
Cu-Cl1′	2.978(1)/2.947(1)	2.689(1)	C4–N5	1.306(4)/1.309(4)	1.367(5)
C6–O7		1.225(6)	N5–C6	1.468(4)/1.469(4)	1.359(5)
Angles (°)					
S1–Cu–N5	95.4(1)/96.0(1)	93.3(1)	N(5)–Cu–Cl1′	87.2(1)/82.7(1)	96.2(1)
N5–Cu–N56	83.0(1)/83.0(1)	81.2(1)	N(56)–Cu–Cl1′	84.4(1)/91.2(1)	96.0(1)
N56–Cu–Cl	93.8(1)/94.3(1)	94.8(1)	S(1)–Cu–Cl1′	105.6(1)/99.1(1)	105.1(1)
Cl–Cu–S1	88.1(1)/87.0(1)	88.4(1)	Cl–Cu–Cl1′	91.1(1)/96.1(1)	89.9(1)
S1–Cu–N56	169.8(1)/169.5(1)	158.7(1)	Cu–Cl–Cu1′	88.9(1)/83.9(1)	90.1(1)
N5–Cu–Cl	176.5(1)/176.9(1)	173.0(1)			

Symmetry transformations used to generate equivalent atoms: for **3a** (1 − x, 1 − y, −z)/(1 − x, −y, 1 − z), (′) for **4a** (−x, −y + 2, −z).

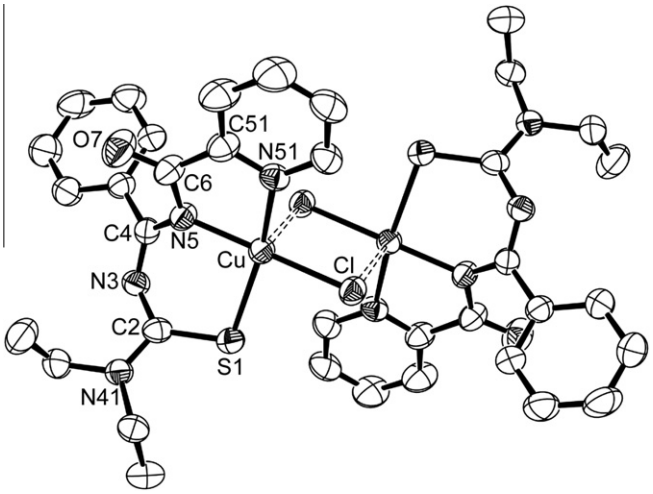

Fig. 4. ORTEP representation of **4a** (50% thermal ellipsoids) [22]. Hydrogen atoms have been omitted for clarity.

square basal plane by about 0.2 Å. The Cu atom is placed about 0.254(2) Å above the plane defined by the three donor atoms S1, N5, N56 of the organic ligand $\{^{*}L\}^{-}$ and one chlorido ligand towards the apical bridging chlorido ligand. The six membered benzamidine chelate ring in **4a** is significantly distorted (with a maximum distortion of 0.322(3) Å for N5 atom). This is in good agreement with unequal distances of the C–N bonds in the benzamidine chelate ring, in which the C4–N3 bond with a length of 1.294(5) Å is considerably shorter and reflects more double bond character than the other C–N bonds. The C6-O7 bond distance of 1.225(6) Å is within the typical range of carbon–oxygen double bonds. Conjugation between this carbonyl group and the adjacent nitrogen atom N5 is also found and indicated by the N5-C6 bond length of 1.359(5) Å, which is significantly shorter than the corresponding bond in **3a**. Some other selected bond lengths and angles of **4a** are compared to those of **3a** in Table 2.

It is well-known that the cytotoxic properties of a bioactive ligand can be influenced by chelate formation. Several mechanisms of antitumor activity of metal complexes have been proposed. Changed activity of a thermodynamically stable and kinetically inert metal complex is due to the difference in the nature of molecules, while that of labile metal complexes may be assigned to the effect of a metal-assisted transport and consequent complex dissociation inside the cell which releases the biologically active species. We investigated the antiproliferative effects of the ligands HL^{R}, their complexes with different metal ions (compounds **1–3**) and complexes **4** on human MCF-7 breast cancer cells in a concentration response assay. This allows the determination of their IC_{50} values. In the cell, compounds **3** and **4** can undergo ligand exchange reactions, during which the very weak and labile Cu–Cl′ bond is primarily cleaved by interaction with biological ligands. Thus, the IC_{50} values of **3** and **4** are reported based on the concentration of their monomeric complexes. The compounds HL^{R} only cause a very weak reduction of the growth of human MCF-7 breast cancer cells. Although the IC_{50} value of HL^{Morph} (94 μM) is much lower than that of HL^{Et} (>400 μM), this value is still far too high for a promising bioactive substance. The complexation of HL^{R} with metal ions is expected to increase the cytotoxicity of the compound. In fact, all the complexes of HL^{R} studied herein exhibit IC_{50} values, which are lower than those of the free ligands (Table 3). The Ni(II) and Pd(II) complexes have IC_{50} values higher than 70 μM, reflecting low cytotoxicity. While the antiproliferative effect of $[Ni(L^{Et})Cl]$ is stronger than that of $[Pd(L^{Et})Cl]$, the activities of the two $\{L^{Morph}\}^{-}$ complexes **1b** and **2b** are similar. For the Ni(II) and Pd(II) complexes, the IC_{50} values of the complexes with $\{L^{Morph}\}^{-}$ are lower than those with $\{L^{Et}\}^{-}$. Surprisingly, the replacement of the metal ion by Cu(II) in **3** results in a dramatic decrease of their IC_{50} values (**3a**: IC_{50} = 0.42; **3b**: IC_{50} = 1.14), which are much lower than that of cisplatin (IC_{50} = 7.10, determined under the same experimental conditions) [18]. This is particularly interesting due to the fact that the uncomplexed Cu^{2+} ion has almost no effect on the growth of MCF-7 cancer cells [19]. Additionally, the structural effect of the dimeric form of **3** can be excluded due to the very weak bridging Cu–Cl′ bond which should be readily cleaved during exchange reactions with plasma components. Under the conditions present in the cytotoxicity assay, however, the oxidation of complexes **3** by oxygen to **4** cannot be excluded. Thus, the cytotoxic effects of **4** were additionally studied. The obtained results show very compatible IC_{50} values between the respective complexes **3** and **4**, which strongly suggests that oxidation of complexes **3** occurs during the determination of the cytotoxicity. For the Cu(II) complexes of these new ligand systems, the replacement of the Morph substituent (**4b**: IC_{50} = 1.05) by an *N,N*-diethyl group (**4a**: IC_{50} = 0.40) increases the activity by more than a factor 2.

The interesting cytotoxic properties of **4** should involve the nature of the new ligand framework $\{^{*}L^{R}\}^{-}$ and it will be worth studying the bioactivity of these ligands as well as their complexes with other metal ions. However, up until now all our attempts to isolate reasonable amounts of pure $H^{*}L^{R}$ by the decomposition of **4** with H_2S failed. Currently, we are trying to synthesize larger amounts of $H^{*}L^{R}$ directly from the reaction of benzimidoyl chloride. The bioactivity of these ligands and their metal complexes will be studied in the future.

Table 3
Cytotoxic effects of the ligands HL and their complexes against MCF-7 Cells.

	IC_{50} (μM)				
	HL^{R}	$[Ni(L^{R})Cl]$	$[Pd(L^{R})Cl]$	$[Cu(L^{R})Cl]$	$[\{Cu(^{*}L^{R})Cl\}_2]$
R = Et	>400	117	274	0.42	0.40
R = Morph	94	75	76	1.14	1.05

3. Experimental

3.1. Materials

All reagents used in this study were reagent grade and used without further purification. Solvents were dried and freshly distilled prior to use unless otherwise stated. $[PdCl_2(MeCN)_2]$ was synthesized by a literature procedure [20].

3.2. Physical Measurements

Infrared spectra were measured as KBr pellets on a Shimadzu FTIR-spectrometer between 400 and 4000 cm^{-1}. Positive ESI mass spectra were measured with an Agilent 6210 ESI–TOF. All MS results are given in the form: *m/z*, assignment. Elemental analysis of carbon, hydrogen, nitrogen and sulfur were determined using a Heraeus vario EL elemental analyzer. Electronic spectra were measured in $CHCl_3$ with a Shimadzu UV-1650PC.

3.3. Preparation of the ligands

The *N*-(dialkylthiocarbamoyl)-*N*′-picolylbenzamidines were prepared following our previously published procedure with slight modifications [4]. *N*-(*N*′,*N*′-Dialkylylaminothiocarbonyl)-benzimidoyl chloride (4 mmol) was added to a mixture containing picolylamine (4 mmol) and Et_3N (12 mmol) in 10 mL of dry THF.

The mixture was stirred for 3 h at room temperature. The colorless precipitate of NEt_3·HCl was filtered off, and the solvent of the filtrate was removed under reduced pressure. The residue was dissolved in 5 mL of a MeOH/diethyl ether mixture (1/1) and stored at −20 °C. The colorless solid of H_2L, which deposited from this solution, was filtered off, washed with diethyl ether, and dried under vacuum.

3.3.1. Data for HL^{Et}

Yield: 85% (1.108 g). Elemental analysis: Calc. for $C_{18}H_{22}N_4S$: C, 66.22; H, 6.79; N, 17.16; S, 9.82. Found: C, 65.72; H, 6.58; N, 16.82; S, 9.05%. IR (KBr, cm^{-1}): 3217 (m), 3065 (m), 2980 (w), 2928 (w), 1608 (vs), 1582 (s), 1535 (s), 1482 (s), 1355 (m), 1292 (s), 1254 (m), 1112 (s), 1080 (m), 1025 (m), 946 (w), 925 (w), 779 (m), 687 (m). ^{1}H NMR (500 MHz, $CDCl_3$, ppm): 1.18 (t, *J* = 7.0 Hz, 3H, CH_3), 1.25 (t, *J* = 7.0 Hz, 3H, CH_3), 3.64 (q, *J* = 7.0 Hz, 2H, CH_2), 3.93 (q, *J* = 7.0 Hz, 2H, CH_2), 4.73 (s, 2H, CH_2-Py), 6.89 (s, br, 1H, NH), 7.21 (t, *J* = 6.1 Hz, 1H, py), 7.38–7.45 (m, 4H, Ph + py), 7.52 (d, *J* = 6.8 Hz, 2H, Ph), 7.70 (t, *J* = 7.5 Hz, 1H, py), 8.53 (d, *J* = 4.8 Hz, 1H, py).

3.3.2. Data for HL^{Morph}

Yield: 70% (0.952 g). Elemental analysis: Calc. for $C_{18}H_{20}N_4OS$: C, 63.50; H, 5.92; N, 16.46; S, 9.42. Found: C, 64.01; H, 5.61; N, 16.42; S, 9.26%. IR (KBr, cm^{-1}): 3215 (m), 3051 (w), 2948 (w), 2894 (w), 2851 (w), 1620 (vs), 1597 (s), 1550 (s), 1435 (m), 1420 (s), 1350 (m), 1308 (s), 1288 (s), 1130 (m), 1112 (s), 1017 (m), 937 (w), 900 (w), 780 (m). ^{1}H NMR (500 MHz, $CDCl_3$, ppm): 3.63 (s, br, 2H, NCH_2), 3.73 (s, br, 2H, NCH_2), 3.81 (s, br, 2H, OCH_2), 4.20 (s, br, 2H, OCH_2), 4.73 (s, 2H, CH_2-Py), 6.93 (s, br, 1H, NH), 7.17 (t, *J* = 6.4 Hz, 1H, py), 7.30–7.38 (m, 4H, Ph + py), 7.45 (d, *J* = 6.8 Hz, 2H, Ph), 7.66 (t, *J* = 7.6 Hz, 1H, py), 8.46 (d, *J* = 4.5 Hz, 1H, py).

3.4. Synthesis of the complexes

*3.4.1. Synthesis of [Ni(L^R)Cl] (**1**)*

$NiCl_2$ 6 H_2O (0.4 mmol) was dissolved in 5 mL of methanol and added to a solution of HL^R (0.4 mmol) in 5 mL methanol. A deep red solution was obtained immediately, which was stirred at room temperature for 15 min and then evaporated slowly to give large red crystals of **1**.

*3.4.1.1. Data for [Ni(L^{Et})Cl] (**1a**).* Yield: 80% (134 mg). Elemental analysis: Calc. for $C_{18}H_{21}ClN_4NiS$: C, 51.52; H, 5.04; N, 13.35; S, 7.64. Found: C, 51.06; H, 5.33; N, 13.72; S, 7.51%. IR (KBr, cm^{-1}): 3075 (w), 2976 (w), 2927 (w), 1503 (vs), 1486 (vs), 1425 (vs), 1347 (m), 1255 (m), 1141 (m), 1074 (m), 760 (w), 708 (w). ^{1}H NMR (500 MHz, $CDCl_3$, ppm): 1.07 (s, br, 3H, CH_3), 1.27 (s, br, 3H, CH_3), 3.55 (m, br, 2H, CH_2), 3.78 (m, br, 2H, CH_2), 4.48 (s, 2H, CH_2-Py), 7.04 (d, br, *J* = 7.0 Hz, 1H, py), 7.22–7.40 (m, 6H, Ph + py), 7.69 (m, br, 1H, py), 8.89 (s, br, 1H, py). ESI(+)MS (*m/z*, assignment): 419 ([M+H]$^+$).

*3.4.1.2. Data for [Ni(L^{Morph})Cl] (**1b**).* Yield: 81% (140 mg). Elemental analysis: Calc. for $C_{18}H_{19}ClN_4NiOS$: C, 49.86; H, 4.42; N, 12.92; S, 7.40. Found: C, 49.70; H, 5.03; N, 13.12; S, 7.35%. IR (KBr, cm^{-1}): 3053 (w), 2961 (w), 2890 (w), 2853 (w), 1509 (vs), 1475 (vs), 1436 (s), 1346 (s), 1265 (m), 1227 (m), 1210 (m), 1115 (m), 1027 (m), 902 (w), 781 (m), 761 (m), 722 (m). ^{1}H NMR (500 MHz, $CDCl_3$, ppm): 3.68 (s, br, 2H, NCH_2), 3.74 (s, br, 2H, NCH_2), 3.81 (s, br, 2H, OCH_2), 4.18 (s, br, 2H, OCH_2), 4.43 (s, 2H, CH_2-Py), 7.07 (d, br, *J* = 7.0 Hz, 1H, py), 7.20–7.40 (m, 6H, Ph + py), 7.72 (m, br, 1H, py), 8.86 (s, br, 1H, py). ESI(+)MS (*m/z*, assignment): 433 ([M+H]$^+$).

*3.4.2. Synthesis of [Pd(L^R)Cl] (**2**)*

[$PdCl_2$(MeCN)$_2$] (0.2 mmol) was dissolved in 5 mL of CH_2Cl_2 and added to a solution of HL^R (0.2 mmol) in 5 mL methanol. After stirring for 5 min at room temperature, three drops of NEt_3 were added. The reaction mixture was stirred for additional 10 min until its brown-yellow color turn to bright yellow. Large yellow crystals of **2** were obtained from the reaction mixture by slow evaporation of the solvent.

*3.4.2.1. Data for [Pd(L^{Et})Cl] (**2a**).* Yield: 78% (73 mg). Elemental analysis: Calc. for $C_{18}H_{21}ClN_4PdS$: C, 46.26; H, 4.53; N, 11.99; S, 6.86. Found: C, 46.04; H, 4.87; N, 12.12; S, 6.77%. IR (KBr, cm^{-1}): 3058 (w), 2983 (w), 2925 (w), 1514 (vs), 1485 (vs), 1457 (vs), 1436 (vs), 1418 (vs), 1350 (s), 1254 (m), 1138 (m), 1075 (m), 772 (w), 713 (w). ^{1}H NMR (500 MHz, $CDCl_3$, ppm): 1.08 (t, 7.0 Hz, 3H, CH_3), 1.29 (t, 7.0 Hz, 3H, CH_3), 3.57 (q, 7.0 Hz, 2H, CH_2), 3.82 (q, 7.0 Hz, 2H, CH_2), 4.83 (s, 2H, CH_2-Py), 7.20 (d, *J* = 8.0 Hz, 1H, py), 7.26–7.45 (m, 6H, Ph + py), 7.78 (t, 8.0 Hz, 1H, py), 9.14 (d, 5.5 Hz, 1H, py). ESI(+)MS (*m/z*, assignment): 469 ([M+H]$^+$).

*3.4.2.2. Data for [Pd(L^{Morph})Cl] (**2b**).* Yield: 80% (77 mg). Elemental analysis: Calc. for $C_{18}H_{19}ClN_4PdOS$: C, 44.92; H, 3.98; N, 11.64; S, 6.66. Found: C, 45.10; H, 4.09; N, 11.32; S, 6.54%. IR (KBr, cm^{-1}): 2954 (w), 2886 (w), 1524 (vs), 1474 (vs), 1426 (s), 1343 (s), 1200 (m), 1115 (m), 1023 (m), 783 (m), 762 (m), 723 (w). ^{1}H NMR (500 MHz, $CDCl_3$, ppm): 3.70 (s, br, 4H, NCH_2), 4.02 (s, br, 4H, NCH_2), 4.84 (s, 2H, CH_2-Py), 7.22 (d, *J* = 8.0 Hz, 1H, py), 7.31(d, *J* = 7.5 Hz, 2H, Ph), 7.35 (t, *J* = 7.0 Hz, 1H, Ph), 7.43–7.48 (m, 3H, Ph + py), 7.80 (t, *J* = 8.0 Hz, 1H, py), 9.16 (d, *J* = 5.5 Hz, 1H, py). ESI(+)MS (*m/z*, assignment): 483 ([M+H]$^+$).

*3.4.3. Synthesis of [{Cu(L^R)Cl}$_2$] (3) and [{Cu($^*L^R$)Cl}$_2$] (**4**)*

The [{Cu(L^R)Cl}$_2$] complexes were prepared following a procedure similar to that for **1**, except that $CuCl_2$ 4H_2O was used instead of nickel chloride. The compounds **3** precipitated directly from the reaction solutions as dark blue crystalline solids. Large dark blue crystals of **3** were obtained by slow diffusion of MeOH into a solution of **3** in CH_2Cl_2 under N_2 atmosphere. Light blue single crystals of **4** were obtained by slow evaporation of a solution of **3** in MeOH/CH_2Cl_2 under aerobic conditions.

*3.4.3.1. Data for [{Cu(L^{Et})Cl}$_2$] (**3a**).* Yield: 78% (132 mg). Elemental analysis: Calc. for $C_{36}H_{42}Cl_2Cu_2N_8S_2$: C, 50.93; H, 4.99; N, 13.20; S, 7.55. Found: C, 51.04; H, 4.80; N, 13.07; S, 7.63%. IR (KBr, cm^{-1}): 3053 (w), 2971 (w), 2928 (w), 1519 (s), 1484 (vs), 1439 (vs), 1411 (vs), 1344 (s), 1257 (m), 1138 (w), 1075 (w), 764 (w), 712 (w). ESI(+)MS (*m/z*, assignment): 424 ([Cu(L^{Et})Cl+H]$^+$), 388 ([Cu(L^{Et})]$^+$). UV–Vis [$CHCl_3$; λ_{max} (nm), ε (dm^3 mol^{-1} cm^{-1})]: 575 (280).

*3.4.3.2. Data for [{Cu(L^{Morph})Cl}$_2$] (**3b**).* Yield: 83% (145 mg). Elemental analysis: Calc. for $C_{36}H_{38}Cl_2Cu_2N_8O_2S_2$: C, 49.31; H, 4.37; N, 12.78; S, 7.31. Found: C, 49.19; H, 4.12; N, 12.85; S, 7.51%. IR (KBr, cm^{-1}): 2910 (w), 2843 (w), 1509 (s), 1470 (vs), 1438 (vs), 1417 (vs), 1342 (s), 1263 (m), 1227 (m), 1205 (m), 1111 (m), 1029 (m), 788 (m), 765 (m). ESI(+)MS (*m/z*, assignment): 438 ([Cu(L^{Morph})Cl+H]$^+$), 402 ([Cu(L^{Morph})]$^+$). UV–Vis [$CHCl_3$; λ_{max} (nm), ε (dm^3 mol^{-1} cm^{-1})]: 574 (273).

*3.4.3.3. Data for [{Cu($^*L^{Et}$)Cl}$_2$] (**4a**).* Elemental analysis: Calc. for $C_{36}H_{38}Cl_2Cu_2N_8O_2S_2$: C, 49.31; H, 4.37; N, 12.78; S, 7.31. Found: C, 49.15; H, 4.41; N, 12.90; S, 7.50%. IR (KBr, cm^{-1}): 3059 (w), 2972 (w), 2932 (w), 1661 (vs), 1584 (s), 1568 (vs), 1525 (vs), 1446 (m), 1352 (vs), 1307 (m), 1280 (m), 1244 (m), 1136 (w), 1078 (w), 760 (w), 703 (w). ESI(+) MS (*m/z*, assignment): 438

Table 4
Crystal data and structure refinement parameters.

	1a	1b	2a	3a	4a
Formula	$C_{18}H_{21}ClN_4NiS$	$C_{18}H_{19}ClN_4NiOS$	$C_{18}H_{21}ClN_4PdS$	$C_{18}H_{21}ClCuN_4S$	$C_{18}H_{19}ClCuN_4OS$
M_w	419.61	433.59	467.30	424.44	438.44
Crystal system	monoclinic	triclinic	triclinic	triclinic	monoclinic
a (Å)	8.086(1)	9.053(1)	12.645(1)	11.713(1)	8.928(1)
b (Å)	19.600(1)	11.073(1)	12.923(1)	11.916(1)	21.334(1)
c (Å)	12.224(1)	19.911(1)	14.283(1)	17.001(1)	10.287(1)
α (°)	90	87.25(1)	64.46(1)	75.85(1)	90
β (°)	105.75(1)	83.64(1)	66.83(1)	70.00(1)	99.16(1)
γ (°)	90	66.78(1)	71.94(1)	60.70(1)	90
V (Å^3)	1864.6(3)	1823.0(3)	1908.1(2)	1935.9(3)	1934.4(3)
Space group	$P2_1/n$	$P\bar{1}$	$P\bar{1}$	$P\bar{1}$	$P2_1/n$
Z	4	4	4	4	4
D_c (g cm^{-3})	1.495	1.580	1.627	1.456	1.505
μ (mm^{-1})	1.304	1.341	1.230	1.382	1.389
No. of reflections	12692	22325	21463	21035	14044
No. of independent	4985	9810	10214	10351	5160
No. parameters	227	470	452	451	236
R_1/wR_2	0.0549/0.1434	0.0500/0.1258	0.0677/0.1284	0.0463/0.0965	0.0583/0.1315
Goodness-of-fit	1.002	0.939	0.944	0.949	0.962

([Cu($^*L^{Et}$)Cl+H]$^+$). UV–Vis [$CHCl_3$; λ_{max} (nm), ε (dm^3 mol^{-1} cm^{-1})]: 601 (157).

*3.4.3.4. Data for [{Cu($^*L^{Morph}$)Cl}$_2$] (**4b**).* Elemental analysis: Calc. for $C_{36}H_{34}Cl_2Cu_2N_8O_4S_2$: C, 47.79; H, 3.79; N, 12.38; S, 7.09. Found: C, 48.04; H, 3.53; N, 12.32; S, 7.01%. IR (KBr, cm^{-1}): 3065 (w), 2997 (w), 2856 (w), 1658 (vs), 1584 (s), 1562 (vs), 1523 (s), 1447 (m), 1358 (vs), 1308 (m), 1278 (m), 1250 (m), 1141 (w), 1110 (w), 1026 (w), 762 (w), 703 (w). ESI(+) MS (*m/z*, assignment): 452 ([Cu($^*L^{Morph}$)Cl+H]$^+$). UV–Vis [$CHCl_3$; λ_{max} (nm), ε (dm^3 mol^{-1} cm^{-1})]: 603 (150).

3.5. X-ray crystallography

The intensities for the X-ray determinations were collected on a STOE IPDS 2T instrument with Mo Kα radiation (λ = 0.71073 Å). Standard procedures were applied for data reduction and absorption correction. Structure solution and refinement were performed with SHELXS-97 and SHELXL-97 [21]. Hydrogen atoms were calculated for idealized positions and treated with the 'riding model' option of SHELXL [21].

More details on data collections and structure calculations are contained in Table 4. Additional information on the structure determinations has been deposited with the Cambridge Crystallographic Data Centre.

3.6. In vitro cell tests

The cytotoxic activity of the compounds was determined using MTT assay. Human cancer cells of the cell line MCF-7 were obtained from the American Type Culture Collection (Manassas, VA) ATCC. Cells were cultured in medium RPMI 1640 supplemented with 10% FBS (Fetal bovine serum) under a humidified atmosphere of 5% CO_2 at 37 °C. The testing substances were initially dissolved in DMSO then diluted to the desired concentration by adding cell culture medium. The samples (100 μL) of complexes with different concentrations were added to the wells on 96-well plates. Cells were detached with trypsin and EDTA and seeded in each well with 3×10^4 cells per well. After incubation for 48 h, a MTT solution (20 μL, 4 mg mL^{-1}) of phosphate buffer saline (8 g NaCl, 0.2 g KCl, 1.44 g Na_2HPO_4 and 0.24 g KH_2PO_4/L) was added into each well. The cells were further incubated for 4 h and a purple formazan precipitate was formed, which was separated by centrifugation. DMSO (100 μL) was added to each well to dissolve the precipitate. The optical density of the solution was determined by a plate reader (TECAN) at 540 nm. The inhibition ratio was calculated on the basis of the optical densities obtained from three replicate tests.

Acknowledgement

We thank Vietnam's National Foundation for Science and Technology Development for financial support through Project 104.02–2010.31.

Appendix A. Supplementary data

CCDC 881132 (**1a**), 881130 (**1b**), 881131 (**2a**), 881133 (**3a**) and 881134 (**4a**) contain the supplementary crystallographic data. These data can be obtained free of charge via http://www.ccdc.cam.ac.uk/conts/retrieving.html, or from the Cambridge Crystallographic Data Centre, 12 Union Road, Cambridge CB2 1EZ, UK; fax: +44 1223 336 033; or e-mail: deposit@ccdc.cam.ac.uk.

References

[1] L. Beyer, R. Widera, Tetrahedron Lett. 23 (1982) 1881.
[2] L. Beyer, J. Hartung, R. Widera, Tetrahedron 40 (1984) 405.
[3] (a) J. Hartung, G. Weber, L. Beyer, R. Szargan, Z. Anorg. Allg. Chem. 523 (1985) 153;
(b) R. del Campo, J.J. Criado, E. Garcia, M.R. Hermosa, A. Jimenez-Sanchez, J.L. Manzano, E. Monte, E. Rodriguez-Fernandez, F. Sanz, J. Inorg. Biochem. 89 (2002) 74;
(c) W. Hernandez, E. Spodine, R. Richter, K.H. Hallmeier, U. Schröder, L. Beyer, Z. Anorg. Allg. Chem. 629 (2003) 2559;
(d) U. Schröder, R. Richter, L. Beyer, J. Angulo-Cornejo, M. Lino-Pacheco, A. Guillen, Z. Anorg. Allg. Chem. 629 (2003) 1051;
E. Guillon, I. Dechamps-Olivier, A. Mohamadou, J-P. Barbier, Inorg. Chim. Acta 268 (1998) 13;
(f) R. Richter, U. Schröder, M. Kampf, J. Hartung, L. Beyer, Z. Anorg. Allg. Chem. 623 (1997) 1021.
[4] H.H. Nguyen, J. Grewe, J. Schroer, B. Kuhn, U. Abram, Inorg. Chem. 47 (2008) 5136.
[5] H.H. Nguyen, K. Hazin, U. Abram, Eur. J. Inorg. Chem. (2011) 78.
[6] H.H. Nguyen, V.M. Deflon, U. Abram, Eur. J. Inorg. Chem. 21 (2009) 3179.
[7] H.H. Nguyen, P.I.da S. Maia, V.M. Deflon, U. Abram, Inorg. Chem. 48 (2009) 25.
[8] H.H. Nguyen, J.J. Jegathesh, P.I. da S. Maia, V.M. Deflon, R. Gust, S. Bergemann, U. Abram, Inorg. Chem. 48 (2009) 9356.
[9] J. Schroer, U. Abram, Polyhedron 33 (2012) 218.
[10] (a) R. Richter, J. Sieler, L. Beyer, A.I. Yanovskii, Y.T. Struchkov, Z. Anorg. Allg. Chem. 570 (1989) 84;
(b) F. Lessmann, L. Beyer, K.-H. Hallmeier, R. Richter, J. Sieler, P. Strauch, A. Voigt, Z. Naturforsch. B55 (2000) 253.
[11] P.I. da S. Maia, H.H. Nguyen, D. Ponader, A. Hagenbach, S. Bergemann, R. Gust, V.M. Deflon, U. Abram, Inorg. Chem. 51 (2012) 1604.
[12] H.H. Nguyen, U. Abram, Inorg. Chem. 46 (2007) 5310.

[13] O.A. Blackburn, B.J. Coe, J. Fielden, M. Helliwell, J.J.W. McDouall, M.G. Hutchings, Inorg. Chem. 49 (2010) 9136.
[14] D.R. Lide (Ed.), CRC Handbook of Chemistry and Physics, 84th ed., CRC Press, 2004.
[15] B.J. Hathaway, Copper, in: G. Wilkinson, R.D. Gillard, J.A. McCleverty (Eds.), Comprehensive Coordination Chemistry, vol. 5, Pergamon Press, 1987, p. 534.
[16] (a) L.M. Fostiak, I. García, J.K. Swearingen, E. Bermejo, A. Castineiras, D.X. West, Polyhedron 22 (2003) 83;
(b) D.X. West, J.K. Swearingen, A.K. El-Sawaf, Transition Met. Chem. 25 (2000) 87.
[17] S. Roy, P. Mitra, A.K. Patra, Inorg. Chim. Acta 370 (2011) 247.
[18] L. Yan, X. Wang, Y. Wang, Y. Zhang, Y. Li, Z. Guo, J. Inorg. Biochem. 106 (2012) 46.
[19] R.L. Jessica, Z. Xiao-Xi, Z. Jie, D. Wei-Qun, Anticancer Res. 30 (2010) 3249.
[20] P. Pratihar, S. Jha, T.K. Mondal, G. Mostafa, C. Sinha, Polyhedron 26 (2007) 4328.
[21] G.M. Sheldrick, SHELXS-97 and SHELXL-97 Programs for the Solution and Refinement of Crystal Structures, University of Göttingen, Göttingen, Germany, 1997.
[22] L.J. Farrugia, J. Appl. Crystallogr. 30 (1997) 565.